# Temperature-dependent rotationally inelastic collisions of math xmlns="http://www.w3.org/1998/Math/MathML">msup>mrow>mi>OH/mi>/mrow>mo>−/mo>/msup>/math> and He

Eric S. Endres, Steve Ndengué, Olga Lakhmanskaya, Seunghyun Lee, Francesco A. Gianturco, Richard Dawes, and Roland Wester

# Temperature-dependent rotationally inelastic collisions of OH$^-$ and He

Eric S. Endres[1], Steve Ndengué[2,3], Olga Lakhmanskaya[1], Seunghyun Lee[1], Francesco A. Gianturco[1], Richard Dawes[2], and Roland Wester[1*]

[1]*Institut für Ionenphysik und Angewandte Physik, Universität Innsbruck, Technikerstrasse 25/3, 6020 Innsbruck, Austria*

[2]*Department of Chemistry, Missouri University of Science and Technology, 65409 Rolla, Missouri, United States. and*

[3]*ICTP-East African Institute for Fundamental Research, University of Rwanda, Kigali, Rwanda*

(Dated: April 28, 2021)

We have studied the fundamental rotational relaxation and excitation collision of OH$^-$ $J = 0 \leftrightarrow 1$ with helium at different collision energies. Using state-selected photodetachment in a cryogenic ion trap, the collisional excitation of the first excited rotational state of OH$^-$ has been investigated and absolute inelastic collision rate coefficients have been extracted for collision temperatures between 20 and 35 K. The rates are compared with accurate quantum scattering calculations for three different potential energy surfaces. Good agreement is found within the experimental accuracy, but the experimental trend of increasing collision rates with temperature is only in part reflected in the calculations.

## I. INTRODUCTION

Experimental advances in the preparation of ensembles of cold and ultracold molecules have enriched the field of cold chemistry with studies of inelastic and reactive scattering at low temperatures [1–3]. Low temperatures enable rotational state control for molecules and reveal quantum properties of collisions, such as orbiting and shape resonances [4, 5]. Furthermore, control over molecular states has potential applications in fundamental precision studies [6–10], quantum information processing [11, 12] and many-body physics [4, 13].

Cooling molecules, unlike atoms, implies freezing of the internal degrees of freedom. For molecular ions the general way to relax all degrees of freedom is collisional dissipation of energy using buffer gas cooling [14–18]. In standard cryostats, temperatures are limited to above 3 K. Lower temperatures may be reached in hybrid atom-ion-traps, where a magneto-optical trap for ultracold atoms is superimposed with an ion trap [15]. Understanding the rotational quenching kinetics and, more specifically, state-specific inelastic collision rates is necessary to be able to control and manipulate the internal state population of trapped molecular ions.

Inelastic collision studies are also of great relevance for astrophysics, to model relaxation kinetics in the early universe or to describe molecular excitation levels in interstellar molecular clouds [19, 20]. This is particularly important when local thermodynamic equilibrium (LTE) cannot be assumed. Rate coefficients for rotationally inelastic collisions are needed to bring the predicted line intensities into agreement with astronomical observations or to quantitatively correlate deuterium to hydrogen abundance ratios with the conditions in astrophysical environments [21]. Rotational state control is also needed for state-selected ion-molecule reaction studies in order to better understand the gas phase ion chemistry that dominates in cold interstellar clouds [22].

Given their importance, numerous theoretical calculations provide rate coefficients for inelastic rotational state-changing collisions of molecular ions, e.g. for NO$^+$ [23], C$_6$H$^-$ [24], H$_2^+$ [25], or C$_2$H$^-$ and C$_2$N$^-$ [26]. However, only few experiments have been able to provide absolute rate coefficients, in particular at low temperatures. Schlemmer *et al.* have investigated rotational cooling of N$_2^+$ colliding with Argon using a laser-induced reaction [27]. Hansen *et al.* have studied rotational cooling, but did not extract absolute rate coefficients [28]. In Ref. [29] we have introduced a novel scheme to measure inelastic collision rate coefficients via state-specific photodetachment, which is applicable to negatively charged molecules. With this we have obtained the inelastic collision rate coefficients that link the two lowest rotational states of OH$^-$ and OD$^-$ anions in collisions with He.

Here we present experimental results for the temperature dependence of the rotationally inelastic collision rate coefficient of OH$^-$($^1\Sigma^+$) colliding with He using state-specific photodetachment [29]. We use the experimental results to benchmark three different quantum scattering calculations. OH$^-$ is particularly well suited for such studies due to the simple rotational structure in its $^1\Sigma^+$ ground rotational state, the large rotational constant of 562 GHz [30]) and the well studied properties of near threshold photodetachment [31–34].

## II. EXPERIMENTAL PROCEDURE

A detailed description of the experimental set up can be found elsewhere [35, 36]. OH$^-$ anions are produced in a plasma discharge of a helium water mixture and are loaded in a 22-pole radiofrequency ion trap after mass selection. The trap is filled with He buffer gas, which collisionally thermalizes the kinetic ion temperatures and internal degrees of freedom. Buffer gas temperature was varied from 9 K to 30 K. The lifetime of the ions typi-
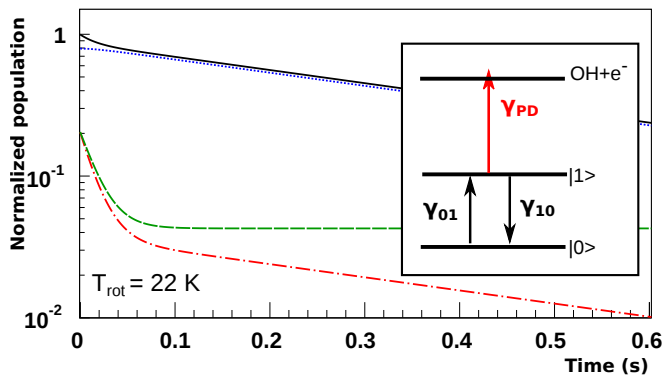
FIG. 1. Time evolution of the rotational state population of $OH^-$ at $22\,K$ rotational temperature. The blue line represents the ground state population $N_0$ and the red line the excited state population $N_1$. The black and green lines show the total population $N_0 + N_1$ and the fraction $N_1/(N_0 + N_1)$, respectively. The graph was simulated with the parameters $\gamma_{PD} = 50\,s^{-1}$ and $\gamma_{10} = 10\,s^{-1}$. The inset illustrates the relevant states and the rates that couple them.

cally exceeds thousands of seconds, and thus, does not affect our measurements. After a short thermalization period, the photodetachment laser is admitted into the trap with powers between $70\,mW$ and $210\,mW$. This initiated the ion losses with rates ranging from $0.2\,s^{-1}$ to about $2\,s^{-1}$. The laser position was tuned to maximize the photodetachment loss rate and thereby the overlap to the trapped ion cloud. As only relative detachment losses are analyzed in the following, a quantitative characterisation of the overlap between laser and ion cloud does not need to be known. The interaction time with the laser was regulated using a self-built mechanical laser shutter.

In the ion trap, $OH^-$ ions undergo collisions with the buffer gas, which couples the rotational states of $OH^-$ via inelastic collisions and establishes a Boltzmann distribution of the rotational level population at a given temperature. The admission of the photodetachment (PD) laser to the trap initiates the loss of ions from the excited rotational state $J = 1$ and higher with a rate $\gamma_{PD}$ (see inset in Fig. 1). Due to the presence of inelastic collisional coupling of the rotational state $J = 0$ and $J = 1$ through the thermal collision rates $\gamma_{01}$ and $\gamma_{10}$, the first excited rotational state gets repopulated. Thus the absolute number of anions in the ground state decays as well. For low enough buffer gas density and high enough laser power this coupling becomes insufficient to maintain the original thermal distribution of the rotational state populations. This leads to a non-linear dependence of the ion losses on laser power.

The time evolution of the rotation state population is calculated by solving the coupled rate equations

$$\frac{d}{dt}\begin{pmatrix} N_0 \\ N_1 \end{pmatrix} = \begin{pmatrix} -\gamma_{01} & \gamma_{10} \\ \gamma_{01} & -(\gamma_{10} + \gamma_{PD}) \end{pmatrix} \begin{pmatrix} N_0 \\ N_1 \end{pmatrix}. \quad (1)$$

Here $OH^-$ is approximated as a two-level system with

populations $N_0$ (ground state) and $N_1$ (excited state). This is a good approximation in the considered temperature range due to the large rotational constant of $OH^-$. The sum of the two equations provides the instantaneous loss rate of the ions

$$\gamma_L(t) = \frac{1}{(N_0 + N_1)}\frac{d}{dt}(N_0 + N_1) = -\frac{N_1}{N_0 + N_1}\gamma_{PD} \quad (2)$$

The rate is time-dependent as the relative population of the excited state changes with time, which leads in general to a non-exponential decay of the trapped ion number. This is shown in Fig. 1, which presents a solution of Eq. (1) for the case of a high photodetachment rate compared to the inelastic relaxation rate. The figure shows the general result of a fast initial relaxation of the relative excited state population $\frac{N_1}{N_0+N_1}$ on a time scale $\tau \sim 1/(\gamma_{01} + \gamma_{10} + \gamma_{PD})$ after which it stays constant. For times $t \gg \tau$ one can simplify the solution of Eq. (2) to an exponential decay with a constant loss rate

$$\gamma_L(t \to \infty) = \frac{2\gamma_{01}\gamma_{PD}}{\gamma_{01} + \gamma_{10} + \gamma_{PD} + \sqrt{(\gamma_{01} + \gamma_{10} + \gamma_{PD})^2 - 4\gamma_{01}\gamma_{PD}}} \quad (3)$$

When the collisional coupling of rotational states is strong compared to the photodetachment rate ($\gamma_{PD} \ll \gamma_{01}, \gamma_{10}$), the ratio $\frac{N_1}{N_0+N_1}$ stays constant. As a result $\gamma_L$ increases linearly with $\gamma_{PD}$ (see. eq. 2).

The thermal excitation and de-excitation rate coefficients are coupled by detailed balance, $\gamma_{01}/\gamma_{10} = g_1/g_0 \exp(-\Delta E/k_B T_{rot})$, to the temperature $T_{rot}$ that describes the rotational population ($g_{0,1}$ are the respective degeneracy factors). This temperature also represents the collision temperature in the center of mass frame of the $OH^-$/He system[18]. It is determined independently at a low photodetachment rate following the rotational thermometry scheme described in Ref. [35]. Due to radiofrequency heating of the ions in the trap this rotational and collisional temperature is slightly larger than the helium buffer gas temperature [36]. Evidence for radiofrequency heating was also found in Doppler-resolved vibrational overtone spectroscopy of $OH^-$ ions [37].

The photodetachment rate $\gamma_{PD}$ is proportional to the laser power admitted into the trap. It could in principle be determined using an absolute photodetachment cross section measurement [38, 39]. However, here we are only interested in the linear dependence of $\gamma_{PD}$ on the measured laser power $P$ and therefore use a free parameter $\eta$ linking $\gamma_{PD} = \eta P$ [40]. As a consequence two free parameters remain in Eq. (3), $\gamma_{10}$ and $\eta$, that need to be fitted to the experimental data.

To extract the inelastic collision rate coefficient $k_{10}$ from the rate $\gamma_{10}$, the latter is divided by the absolute helium density. The employed densities range between $2.7 \cdot 10^{11}\,cm^{-3}$ and $7 \cdot 10^{11}\,cm^{-3}$. The absolute density

TABLE I. Error budget of the density calibration

| Parameter | Error | Comment |
| --- | --- | --- |
| $p_{He}$ | 10% | reproducibility of the cold cathode gauge |
| $\alpha$ | 2.5% | measured fluctuations over many days |
| $T_T$ | 1% | estimated precision of the employed silicon temperature diodes |
| $T_{out}$ | 0.3% | upper limit to the laboratory temperature fluctuations |

calbration is carried out as described in the supplementary information of Ref. [29]. The density $n$ is calculated using the ideal gas equation from the helium partial pressure $p_{He}$, which measured with a cold cathode gauge in the vacuum chamber,

$$n = \frac{\alpha\, p_{He}}{k_B \sqrt{T_T T_{out}}}. \tag{4}$$

$T_T$ and $T_{out}$ are respectively the cryogenic temperature of the trap and the ambient temperature of the setup, $k_B$ is the Boltzmann constant. The factor $\alpha$ is used to calibrated the cold cathode gauge to an accurate capacitive gauge, which mesaures the pressure directly inside the ion trap, but can only operate at pressures higher than the low helium partial pressures needed in the present experiment. This accounts for the increased particle density inside the cryogenic ion trap compared to the surrounding vacuum chamber.

The contributions to the statistical error of the density originate from the pressure measurement $p_{He}$, the pressure calibration factor $\alpha$, and the two temperature measurements. These contributions are shown in Table I and amount to an overall error of about 15 %. An additional systematic error arises from the presence and the fluctuations of residual helium background gas in the vacuum chamber that has to be subtracted. This error was estimated using a quadrupole mass spectrometer and found to be below 1 % for the present measurements.

## III. THEORETICAL METHODS

### A. Potential energy surface calculations

To precisely calculate the collisional quenching rates of excited rotational states, we have constructed two new potential energy surfaces (PESs), which we compare to an existing PES from our earlier work. The two new PESs are computed using coupled-cluster theory beginning with CCSD(T) at the complete basis set limit and adding the small contribution of electron correlation at the CCSDT(Q) level. The third PES was obtained using MP4 theory and the rigid rotor geometry of the anion [29, 41].

The first new PES (denoted $r_0$) fixes the OH bond distance at the diatomic ground state vibrationally averaged distance. It is calculated at the level of (AE)-CCSD(T)/CBS, where (AE) indicates that all electrons were included in the correlation treatment, and CBS indicates that the complete basis set limit was estimated by extrapolation. Here the aug-cc-pwCVQZ and aug-cc-pwCV5Z bases[42] (each with an even-tempered extension adding $s$, $p$, $d$ and $f$ functions to the standard basis) were extrapolated using the $l^{-3}$ formula. The OH bond distance was fixed at $r_0$=0.974275 Å, a vibrationally averaged value consistent with the experimental rotational constant of the OH$^-$ anion[34]. A computed correction for the contribution of high-order correlation was also added. The correction was defined as the difference between energies at the CCSDT(Q)/AVTZ and CCSD(T)/AVTZ levels. The MOLPRO[43] and CFOUR[44] electronic structure code packages were used for all of the calculations reported here.

The second PES (denoted $v_0$) was constructed by averaging over the diatomic ground state vibrational probability density. It employs the same level of electronic structure theory as the first PES, but uses separate calculations at a series of OH bond distances in order to average over the diatomic ground state vibrational probability density rather than using a single fixed $r_0$ distance. A variational $J = 0$ vibrational calculation was performed for OH$^-$ using the potential optimized discrete variable representation method[45]. This permits an accurate representation of the lowest vibrational state using just three points located at 0.892135, 1.012750, and 1.146084 Å, with respective weights of 0.334001091, 0.605332536 and 0.060666373. In order to minimize fitting errors, three separate 2D PESs were constructed (one for each of the three necessary bond distances) and then the weights were applied to construct the final vibrationally averaged $v_0$ PES.

Both two-dimensional PESs are represented analytically by interpolating high-level ab initio data using the same interpolating moving least squares method used previously for many van-der Waals systems[24, 46–50]. In this application 475 automatically generated geometries were determined in the center of mass distance range of $R$=[1.7,15] Å. The fit represents all attractive regions and repulsive regions up to 2800 cm$^{-1}$ above the separate fragments asymptote. A pruned product basis of 39 functions (Legendre and radial) was used for the interpolation. The estimated fitting error with respect to independent test sets is below 0.01 cm$^{-1}$. To represent the long range, an additional 80 points were computed in the range of $R$=[6,25] Å and fit to a Legendre-based analytic representation. A hyperbolic tangent switching function was used to smoothly switch between the short and long range representations, which was centered at 9.0 Å.

The global minimum of all three employed PESs is found at a collinear configuration with the He atom at the O-atom end of the OH$^-$ molecule. For the highest level
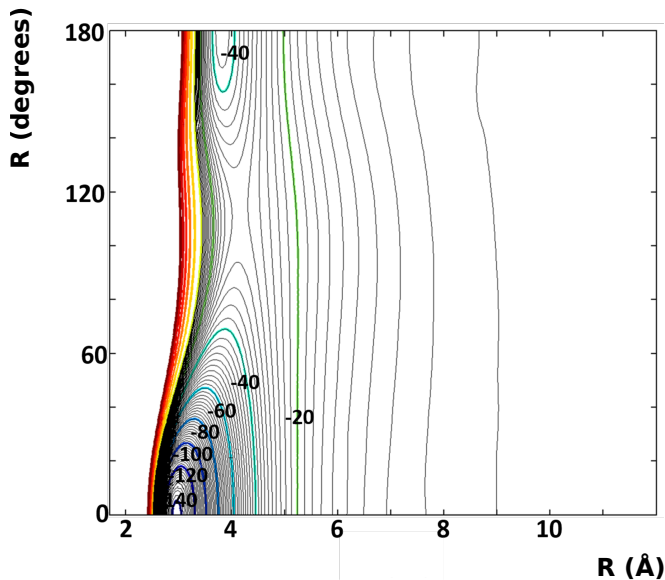
FIG. 2. A plot of the $r_0$ potential energy surface. Black contours appear at 2 cm$^{-1}$ intervals and colored contours (marked with numbers) every 20 cm$^{-1}$.

$v_0$ PES, the geometry of the global minimum is $R$=2.691 Å, $\theta$=0$^o$, $E$=-139.21 cm$^{-1}$. For the $r_0$ PES, the geometry of the global minimum is $R$=2.958 Å, $\theta$=0$^o$, $E$=-140.96 cm$^{-1}$. The corresponding data for the earlier PES have been reported in Refs. [41]. Fig. 2 shows a plot of the $r_0$ PES in Jacobi coordinates. As seen in Fig. 2, a local minimum is found for the other collinear arrangement placing the He atom toward the H-atom. The geometry of the local minimum for the $v_0$ PES is: $R$=3.875 Å, $\theta$=180$^o$, $E$=-38.62 cm$^{-1}$. The geometry of the local minimum for the $r_0$ PES is: $R$=3.809 Å, $\theta$=180$^o$, $E$=-42.13 cm$^{-1}$. The vibrational averaging has a fairly significant impact on the locations of the minima, but a fairly small impact on the well depths.

In order to perform the scattering calculations, the PESs were represented as the radial dependence of a Legendre expansion up to the $8^{th}$ order according to

$$V(R,\theta) = \sum_\lambda v_\lambda(R) \, P_\lambda(\theta), \qquad (5)$$

where $P_\lambda(\theta)$ are the Legendre polynomials. The order of the expansion was confirmed to be sufficient by performing convergence test calculations with an expansion order of 10. The first 4 Legendre coefficients $v_\lambda(R)$ for the $r_0$ PES are plotted in Figures 3a. In Fig. 3b they can be compared to the first 4 Legendre coefficients of the third PES [41] that was used in Ref. [29]. We observe from these figures two immediate differences on the even coefficients of the Legendre expansion. While the $l = 2$ term is less deep in the expansion of the new PESs than it is in the same expansion for Gonzalez-Sanchez $et$ $al$'s[41] PES, the opposite is true for the $l = 0$ coefficient. On the other hand, the odd coefficients, those which dominate the action of the dynamical torque causing excitations during
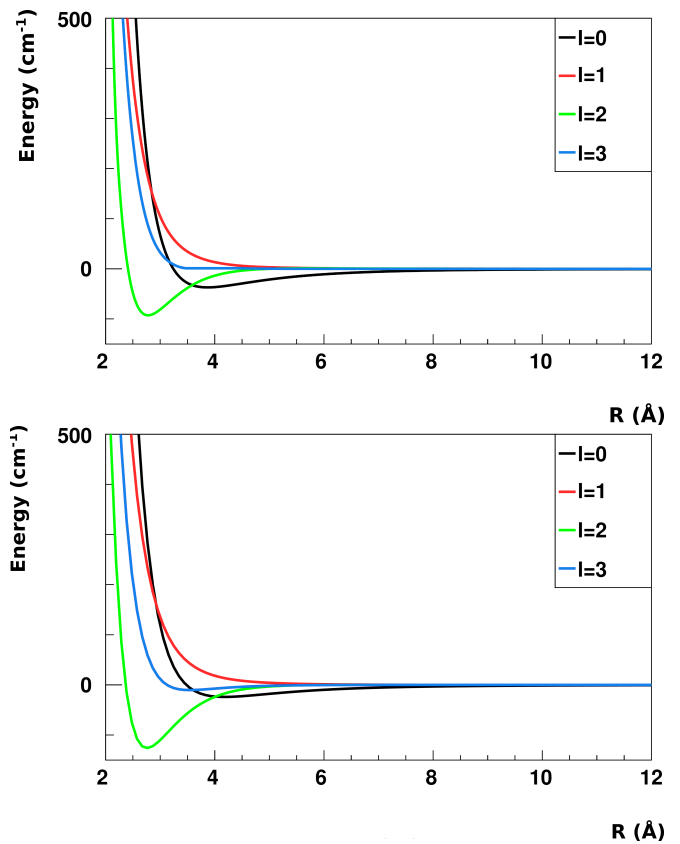


FIG. 3. a) First 4 Legendre expansion functions of the $r_0$ PES for OH$^-$-He. b) Same 4 Legendre expansion functions of the OH$^-$-He PES of Gonzalez-Sanchez $et$ $al$'s[41].

the collisions, are very similar in shape and on their repulsive regions. The fact that the $l = 1$ coefficient is slightly more repulsive for the PES of Fig. 3b than for that of Fig. 3a may well be the cause of finding smaller inelastic cross sections when using the former PES in the calculations.

## B. Scattering calculations

Scattering theory for diatomic molecules is well documented in the literature [51–53]. The time independent collision dynamics calculations where done with the MOLSCAT code [54] for the first two PESs and with the ASPIN code [55] for the third PES. The calculations were performed with the formally exact close coupling method in the $10^{-6} - 10^3$ cm$^{-1}$ energy range.

We verified that, on the same potential, calculations using the MOLSCAT code or the ASPIN code produce the same cross-sections. The MOLSCAT calculations were performed with two different propagators, both yielding the same results: the hybrid modified log-derivative Airy propagator of Alexander and Manolopoulos [56] and the R-matrix propagator of Light and Walker[57]. The results reported here are those from
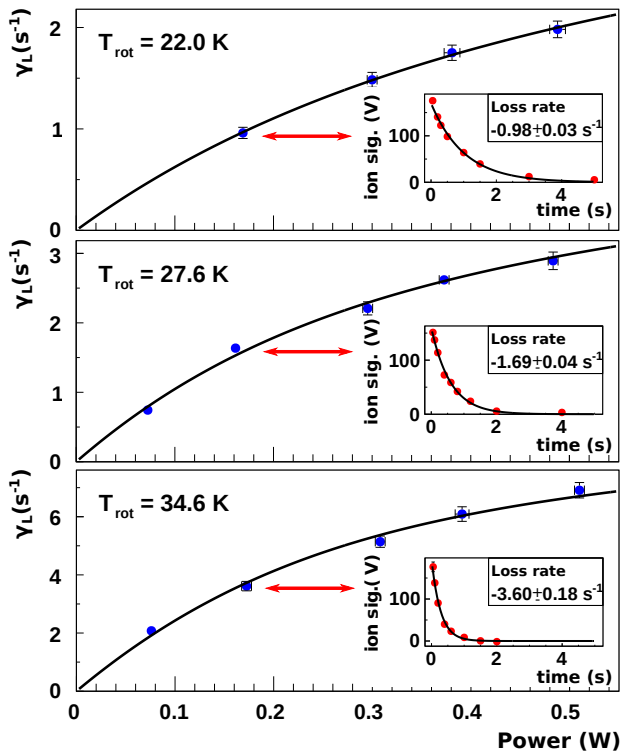
FIG. 4. Power dependent loss rate (blue data points) fitted by the solution to the two level rate equation system (black solid line). The insets show selected individual loss rate measurements. The data have been obtained at trap temperatures that yield the specified rotational temperatures 9 K, 20 K and 30 K [36]. Fit parameters and employed buffer gas densities are reported in Table II.

the R-matrix propagator which was found to complete faster at very low energy than the hybrid modified log-derivative Airy propagator.

The $OH^-$ rotational constant[58] used for the calculation is $B_e = 18.5701 \, cm^{-1}$ with the system reduced mass of $\mu = 3.2399$ a.m.u. . The calculations were done in the $10^{-6} - 10^3 \, cm^{-1}$ energy range. The close coupling calculations are done for every total angular momentum value $J_{tot}$ and converged when the last 4 successive $J_{tot}$ values contribute less than 0.0005 and 0.05 $Å^2$ respectively to the inelastic and elastic cross sections. We used an increasing and sufficient number of basis functions to describe the various energy ranges and ensure convergence of the calculations. A maximum of 11 basis functions for the diatomic rotor, which accounts at 1000 $cm^{-1}$ of collisional energy to 7 open states and 4 closed states, were used in the final calculations. For the earlier PES, the first 11 asymptotic rotational states were included in the coupled channel expansion, thus providing at least four closed channels at the highest energies. Total angular momentum values up to 40 were considered in each computational run. More details are given in Ref. [29, 41].

TABLE II. Results of the inelastic rate fits at different trap temperatures and buffer gas densities.

| $T_{trap}$ [K] | $T_{rot}$ [K] | $\gamma_{10}$ [s$^{-1}$] | $\epsilon_\gamma^{\Delta T}$ [s$^{-1}$] | $\rho$ [cm$^{-3}$] | $k_{10}$ [$10^{-11} \frac{cm^3}{s}$] |
|---|---|---|---|---|---|
| 9 | 22.0(7) | 16.7(20) | 1.3 | $3.4 \cdot 10^{11}$ | 4.9(10) |
| 9 | 22.0(7) | 16.5(31) | 1.2 | $2.4 \cdot 10^{11}$ | 6.9(18) |
| 15 | 25.1(7) | 18.1(16) | 1.2 | $2.6 \cdot 10^{11}$ | 6.9(11) |
| 15 | 24.1(10) | 16.3(30) | 1.5 | $1.8 \cdot 10^{11}$ | 8.9(25) |
| 20 | 27.0(8) | 17.9(16) | 1.2 | $2.3 \cdot 10^{11}$ | 7.9(13) |
| 20 | 27.6(10) | 12.0(9) | 1.0 | $1.6 \cdot 10^{11}$ | 7.5(12) |
| 30 | 33.5(13) | 20.5(18) | 1.6 | $1.9 \cdot 10^{11}$ | 11.0(18) |
| 30 | 34.6(15) | 16.4(12) | 1.3 | $1.3 \cdot 10^{11}$ | 12.6(19) |

## IV. RESULTS AND DISCUSSION

Three sets of measured ion loss rates as a function of the photodetachment laser power are plotted in Fig. 4 for three different trap temperatures. Examples for the observed individual exponential decays are shown in the insets. For each trap temperature the rotational or collision temperature of the $OH^-$ interacting with helium has been determined separately, as explained above. The loss rates show a clear non-linear dependence on the power, indicative of the quenching dynamics of the first excited rotational state. To retrieve the inelastic collision rates we fit Eq. (3) to the experimental data (black solid line). The resulting parameters $\gamma_{10}$ are presented for all eight measurement sets in table II together with their fitted statistical accuracy.

In addition to the statistical accuracy we have estimated the influence of the uncertainty of the measured rotational temperature on the inelastic collision rates: The measured power dependent ion loss rate was fitted assuming different rotational temperatures, namely $T_{rot}$, $T_{rot} + \Delta T_{rot}$ and $T_{rot} - \Delta T_{rot}$. The resulting deviations are deduced to be $\varepsilon_\gamma^{\Delta T} = \frac{1}{2} \cdot |\gamma_{10}(T_{rot} + \Delta T_{rot}) - \gamma_{10}(T_{rot} - \Delta T_{rot})|$. The values are comparable to the statistical accuracy (see Table II).

The measured inelastic collision rates $\gamma_{10}$ depend linearly on the helium buffer gas density [29]. The rate coefficients $k_{10}$, obtained by division through this density, is therefore subject to a larger uncertainty due to the systematic accuracy of the density measurement. As presented in Table I, several sources add up to a relative uncertainty of the density determination of 15 %. The resulting rate coefficients are provided in Table II and in Fig. 6, where they are compared with calculations.

The calculated inelastic cross-sections of the $J = 1 \rightarrow 0$ transition are depicted in Fig. 5 (upper panel) for the three surfaces discussed here. As one can see, the cross sections from the $v_0$ PES are a little smaller than those from the $r_0$ PES, while both deviate significantly from the result from the earlier PES. Specifically, the two former cross sections are larger than the latter, in particular in the low-energy regime. The third cross section also shows stronger modifications due to resonance features, which can be linked to differences in the anisotropic parts
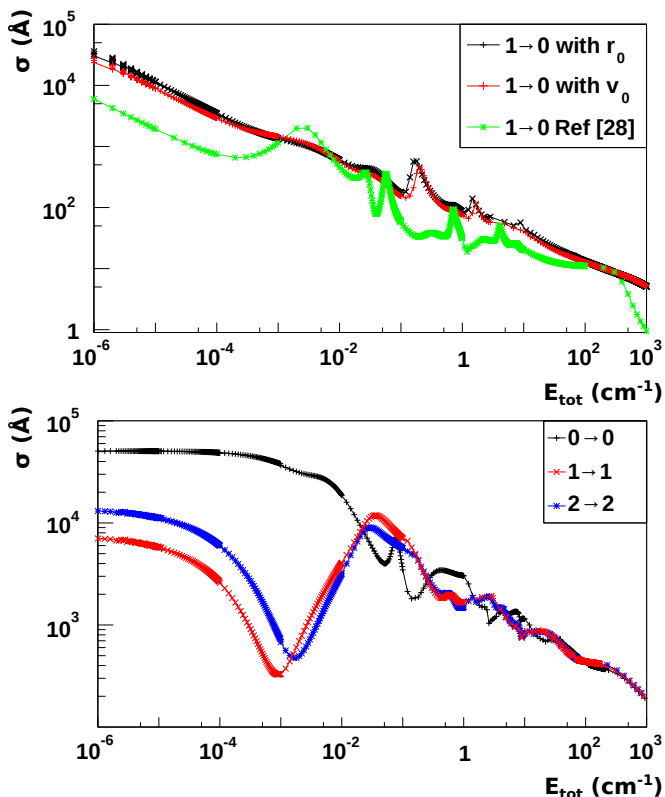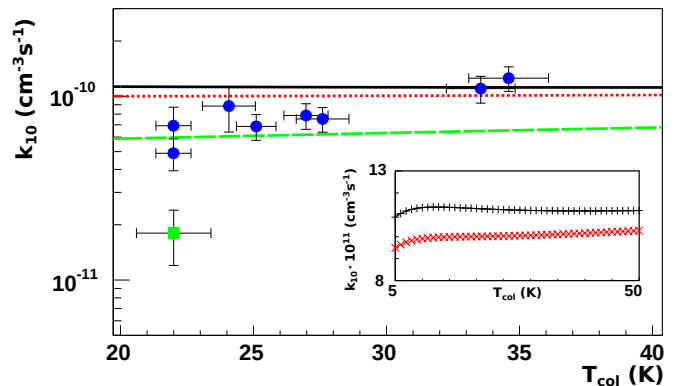
FIG. 6. $J = 1 \rightarrow 0$ inelastic rate coefficients as a function of the collision temperature (blue dots). The green dot shows the measurement from Ref. [29]. The black and red lines show the computational results for the $r_0$ and $v_0$ PESs, respectively, and the green line the theoretical calculation for the earlier PES [29, 41]. The inset shows the calculated rate coefficients for the $r_0$ and $v_0$ PESs over a larger temperature range and on a linear scale.

FIG. 5. Upper panel: Inelastic cross sections for $OH^- + He$ $J = 1 \rightarrow 0$ collisions. The results obtained from the $r_0$ and $v_0$ PESs are compared with the result from the PES from Ref. [29, 41]. Lower panel: Elastic cross sections for $OH^- + He$ collisions in $J=0$, 1 and 2 for the $v_0$ PES.

of the PESs. In addition, Fig. 5 (lower panel) shows elastic cross sections obtained from the $v_0$ PES, for the lowest three rotational states of $OH^-$. These elastic cross sections are about one order of magnitude larger than the inelastic cross section, which is evidence for a more efficient cooling of the translation degrees of freedom compared to rotation. The same type of results have been obtained using the earlier PES [29, 41].

In Fig. 6 the inelastic collision rate coefficients, obtained from thermal averaging of the calculated cross sections with the different PESs, are plotted as a function of the collision temperature and compared to the experimental rate coefficients. In addition, we also present the experimental rate coefficient determined in Ref. [29]. That value is found to be smaller by a factor of three, which corresponds to a little more than $2\sigma$ deviation. While the statistical probability for such a deviation is still finite, we also investigated possible systematic sources of this deviation and found the long-term drift of a calibration factor for the density determination in the previous experiment as a possible source.

Overall the agreement between experiment and theory in Fig. 6 is very favorable. Interestingly, however, all three PESs predict slightly different values for the rate coefficients, differing by almost a factor of two. For the first two PES, the values are significantly larger than the experimental values at low tempreatures up to 30 K, while they agree well for the two measurements around 35 K. The theoretical rates from the earlier PES agree quite well with experiment at the lower temperatures, but are markedly smaller than the experimental values obtained around 35 K. The vibrationally averaged PES produces reduced rate coefficients by about 10% compared to the first PES with fixed bond distance, but this does not markedly change the comparison with the experiment.

The trend of a clear increase of the rate coefficients with temperature is observed in the experiment. This is somewhat captured by the calculations using the earlier PES [29, 41], but it is not reproduced by the new calculations using the $v_0$ and $r_0$ PESs. This shows that rather subtle differences of the interaction potentials lead to observable differences in scattering rates. More accurate potential surface calculations or the explicit inclusion of vibrational excitation in three-dimensional scattering calculations may be needed to resolve this. Additionally, experiments at higher temperatures are desired to shed more light on the true shape of this trend. Ideally, then the next higher rotational state $J = 2$ should also be measured and compared with calculations.

## V. CONCLUSION

In summary, rotational state-selective removal of ions by threshold photodetachment has been applied to measure temperature-dependent inelastic collision rate coefficients of the $OH^-$ anion with helium. A precise analysis of the error budget was carried out including all systematic and statistical error. The experimental data are com-

pared with first-principle theoretical calculations. The present experimental accuracy allowed us to test different rates calculated with three different potential energy surfaces. While in principle a good agreement was found for all the three surfaces, the calculations produced rate coefficients with two different temperature dependences that were both weaker than the measured temperature-dependence. This suggests that more work on the potential surface calculations and comparison of rate coefficients over a broader temperature range are needed in order to gain precise insight in the quantum effects at play.

We expect that the presented progress will also stimulate studies of more complex systems, such as polyatomic and open shell molecules. Recently we already analyzed the collisional quenching kinetics of $NH_2^-$ in helium buffer gas [40], which can be extended to extract inelastic rate coefficients. For the $OH^+(^3\Sigma^-)$ cation, which has been detected in the Orion bar and other interstellar environments, rotational state-selective photodissociation may be used to measure inelastic scattering and test recent quantum inelastic scattering calculations [59].

[1] J. Doyle, B. Friedrich, R. V. Krems, and F. Masnou-Seeuws, Eur. Phys. J. D **31**, 149 (2004).
[2] L. D. Carr, D. DeMille, R. V. Krems, and J. Ye, New J. Phys. **11**, 055049 (2009).
[3] O. Dulieu, R. Krems, M. Weidemüller, and S. Willitsch, Phys. Chem. Chem. Phys. **13**, 18703 (2011).
[4] D. Koch, Cristiane P.; Lemeshko, Michail ; Sugny, Rev. Mod. Phys. **91**, 035005 (2019).
[5] A. Klein, Y. Shagam, W. Skomorowski, P. S. Zuchowski, M. Pawlak, L. M. C. Janssen, N. Moiseyev, S. Y. T. Van De Meerakker, A. Van Der Avoird, C. P. Koch, and E. Narevicius, Nat. Phys. **13**, 35 (2016).
[6] M. S. Safronova, D. Budker, D. DeMille, D. F. J. Kimball, A. Derevianko, and C. W. Clark, Rev. Mod. Phys. **90**, 025008 (2018).
[7] J. J. Hudson, B. E. Sauer, M. R. Tarbutt, and E. A. Hinds, Phys. Rev. Lett. **89**, 023003 (2002).
[8] E. R. Hudson, H. J. Lewandowski, B. C. Sawyer, and J. Ye, Phys. Rev. Lett. **96**, 143004 (2006).
[9] S. Schiller, D. Bakalov, and V. I. Korobov, Phys. Rev. Lett. **113**, 023004 (2014).
[10] M. Germann, X. Tong, and S. Willitsch, Nat. Phys. **10**, 820 (2014).
[11] A. Andre, D. DeMille, J. M. Doyle, M. D. Lukin, S. E. Maxwell, P. Rabl, R. J. Schoelkopf, and P. Zoller, Nat. Phys. **2**, 636 (2006).
[12] D. DeMille, Phys. Rev. Lett. **88**, 067901 (2002).
[13] S. A. Moses, J. P. Covey, M. T. Miecnikowski, D. S. Jin, and J. Ye, Nat. Phys. **13**, 13 (2016).
[14] J. H. V. Nguyen, C. R. Viteri, E. G. Hohenstein, C. D. Sherrill, K. R. Brown, and B. Odom, New J. Phys. **13**, 063023 (2011).
[15] E. R. Hudson, EPJ Techniques and Instrumentation **3**, 8 (2016).
[16] M. Tomza, K. Jachymski, R. Gerritsma, A. Negretti, T. Calarco, Z. Idziaszek, and P. S. Julienne, Rev. Mod. Phys. **91**, 035001 (2019).
[17] S. Willitsch, Int. Rev. Phys. Chem. **31**, 175 (2012).
[18] R. Wester, J. Phys. B **42**, 154001 (2009).
[19] F. Lique and A. Faure, *Gas-Phase Chemistry in Space; From elementary particles to complex organic molecules* (IOP Publishing, 2019).
[20] I. W. M. Smith, Annu. Rev. Astron. Astr. **49**, 29 (2011).
[21] D. Gerlich and S. Schlemmer, Planet. Space Sci. **50**, 1287 (2002), symposium on Deuterium in the Universe, PARIS, FRANCE, JUN 25-27, 2001.
[22] M. Larsson, W. D. Geppert, and G. Nyman, Rep. Prog. Phys. **75**, 066901 (2012).
[23] O. Denis-Alpizar and T. Stoecklin, Mon. Not. R. Astron. Soc. **451**, 2986 (2015).
[24] K. M. Walker, F. Lique, F. Dumouchel, and R. Dawes, Mon. Not. R. Astron. Soc. **466**, 831 (2016).
[25] M. Hernandez-Vera, F. A. Gianturco, R. Wester, H. da Silva Jr, O. Dulieu, and S. Schiller, J. Chem. Phys. **146**, 124310 (2017).
[26] J. Franz, B. Mant, L. González-Sánchez, R. Wester, and F. A. Gianturco, J. Chem. Phys. **152**, 234303 (2020).
[27] S. Schlemmer, T. Kuhn, E. Lescop, and D. Gerlich, Int. J. Mass Spectrom. **185-187**, 589 (1999).
[28] A. K. Hansen, O. O. Versolato, L.Klosowski, S. B. Kristensen, A. Gingell, M. Schwarz, A. Windberger, J. Ullrich, J. R. C. Lopez-Urrutia, and M. Drewsen, Nature **508**, 76 (2014).
[29] D. Hauser, S. Lee, F. Carelli, S. Spieler, O. Lakhmanskaya, E. S. Endres, S. S. Kumar, F. Gianturco, and R. Wester, Nat. Phys. **11**, 467 (2015).
[30] P. Jusko, O. Asvany, A.-C. Wallerstein, S. Brünken, and S. Schlemmer, Phys. Rev. Lett. **112**, 253005 (2014).
[31] P. A. Schulz, R. Mead, P. Jones, and W. Lineberger, J. Chem. Phys. **73**, 1153 (1982).
[32] F. Goldfarb, C. Drag, W. Chaibi, S. Kröger, C. Blondel, and C. Delsart, J. Chem. Phys. **122**, 014308 (2005).
[33] P. C. Engelking and D. R. Herrick, Phys. Rev. A **29**, 2425 (1984).
[34] J. R. Smith, J. B. Kim, and W. C. Lineberger, Phys. Rev. A **55**, 2036 (1997).
[35] R. Otto, A. von Zastrow, T. Best, and R. Wester, Phys. Chem. Chem. Phys. **15**, 612 (2013).
[36] E. S. Endres, G. Egger, S. Lee, O. Lakhmanskaya, M. Simpson, and R. Wester, J. Mol. Spectrosc. **332**, 134 (2017).
[37] O. Lakhmanskaya, M. Simpson, and R. Wester, Phys.

Rev. A **102**, 012809 (2020).

[38] P. Hlavenka, R. Otto, S. Trippel, J. Mikosch, M. Weidemüller, and R. Wester, J. Chem. Phys. **130**, 061105 (2009).

[39] T. Best, R. Otto, S. Trippel, P. Hlavenka, A. von Zastrow, S. Eisenbach, S. Jezouin, R. Wester, E. Vigren, M. Hamberg, and W. D. Geppert, Astrophys. J. **742**, 63 (2011).

[40] F. A. Gianturco, O. Y. Lakhmanskaya, M. Hernández Vera, E. Yurtsever, and R. Wester, Faraday Discuss. **212**, 117 (2018).

[41] L. Gonzalez-Sanchez, F. Marinetti, E. Bodo, and F. A. Gianturco, J. Phys. B **39**, S1203 (2006).

[42] K. A. Peterson and T. H. Dunning Jr, J. Chem. Phys. **117**, 10548 (2002).

[43] H. J. Werner, P. J. Knowles, G. Knizia, F. R. Manby, M. Schütz, *et al.*, "Molpro, version 2012.1, a package of ab initio programs," (2012), see http://www.molpro.net.

[44] CFOUR, a quantum chemical program package written by J.F. Stanton, J. Gauss, L. Cheng, M.E. Harding, D.A. Matthews, P.G. Szalay with contributions from A.A. Auer, R.J. Bartlett, U. Benedikt, C. Berger, D.E. Bernholdt, S. Blaschke, Y.J. Bomble, S. Burger, O. Christiansen, D. Datta, F. Engel, R. Faber, J. Greiner, M. Heckert, O. Heun, M. Hilgenberg, C. Huber, T.-C. Jagau, D. Jonsson, J. Jusélius, T. Kirsch, K. Klein, G.M. Kopper, W.J. Lauderdale, F. Lipparini, T. Metzroth, L.A. Mück, T. Nottoli, D.P. O'Neill, D.R. Price, E. Prochnow, C. Puzzarini, K. Ruud, F. Schiffmann, W. Schwalbach, C. Simmons, S. Stopkowicz, A. Tajti, J. Vázquez, F. Wang, J.D. Watts and the integral packages MOLECULE (J. Almlöf and P.R. Taylor), PROPS (P.R. Taylor), ABACUS (T. Helgaker, H.J. Aa. Jensen,

P. Jørgensen, and J. Olsen), and ECP routines by A. V. Mitin and C. van Wüllen. For the current version, see http://www.cfour.de.

[45] H. Wei and T. Carrington Jr, J. Chem. Phys. **97**, 3029 (1992).

[46] M. Majumder, S. A. Ndengue, and R. Dawes, Mol. Phys. **114**, 1 (2016).

[47] R. Dawes, X.-G. Wang, and T. Carrington Jr, J. Phys. Chem. A **117**, 7612 (2013).

[48] G. Donoghue, X.-G. Wang, R. Dawes, and T. Carrington, J. Mol. Spectrosc. **330**, 170 (2016).

[49] J. Brown, X.-G. Wang, T. Carrington Jr, G. S. Grubbs, and R. Dawes, J. Chem. Phys. **140**, 114303 (2014).

[50] X.-G. Wang, T. Carrington, and R. Dawes, J. Mol. Spectrosc. **330**, 179 (2016).

[51] F. A. Gianturco, *The transfer of molecular energies by collisions: recent quantum treatments* (Springer Verlag, Berlin, 1979).

[52] D. Manolopoulos, J. Chem. Phys. **85**, 6425 (1986).

[53] J. M. Hutson and P. Soldán, Int. Rev. Phys. Chem. **26**, 1 (2007).

[54] J. M. Hutson and C. R. Le Sueur, Comput. Phys. Commun. **241**, 9 (2019).

[55] D. Lopez-Duran, E. Bodo, and F. A. Gianturco, Comp. Phys. Comm. **179**, 821 (2008).

[56] M. H. Alexander and D. E. Manolopoulos, J. Chem. Phys. **86**, 2044 (1987).

[57] J. C. Light and R. B. Walker, J. Chem. Phys. **65**, 4272 (1976).

[58] J. M. Brown and A. Carrington, *Rotational spectroscopy of diatomic molecules* (Cambridge University Press, 2003).

[59] L. González-Sánchez, F. A. Gianturco, and R. Wester, ChemPhysChem **19**, 1866 (2018).